Available online at www.sciencedirect.com
ScienceDirect
Journal of Power Sources 182 (2008) 413–421
JOURNAL OF POWER SOURCES
www.elsevier.com/locate/jpowsour

Polarization study of a PEMFC with four reference electrodes at hydrogen starvation conditions

W.R. Baumgartner*, P. Parz, S.D. Fraser, E. Wallnöfer, V. Hacker

Graz University of Technology, CD-Laboratory for Fuel Cell Systems, Institute for Chemistry and Technology of Inorganic Materials, Steyrergasse 21, 8010 Graz, Austria

Received 31 October 2007; received in revised form 2 January 2008; accepted 2 January 2008
Available online 4 January 2008

Abstract

Hydrogen starvation results in an inhomogeneous distribution of gases within fuel cells and stacks. An inhomogeneous reactant distribution significantly changes the current density distribution over the active cell area and can cause high cathode potentials due to the presence of oxygen in the anode electrode domain. High cathode potentials result in corrosion of the carbon support and thus lead to irreversible cell degradation. A PEMFC single cell assembly was utilised for detailed investigations of these phenomena. The cell was operated with low stoichiometries and in dead-end mode. Product gas analyses were utilised for determining the degradation phenomena.

Keywords: Reference electrode; PEMFC; Electrochemical impedance spectroscopy; Online gas analysis; Gas starvation; Carbon corrosion

1. Introduction

It is inevitably required to detect degradation effects in order to increase the durability of fuel cells. This can only be done by identifying cause and effect of degradation mechanisms, and by preventing the cell from being subject to potentially dangerous operating conditions. Some degradation effects can be studied by exposing small samples to a potentially harmful environments; this is regularly done, e.g. with the development of fuel cell materials. Many degradation effects have to be investigated with engineering-scale single cells and stacks, though [1–3]. Significant variations in local operating conditions are faced in large cells and stacks due to the fact that state-of-the-art gas flow fields consist of a number of individual gas channels. A non-uniform operation of a cell or stack will necessarily result in the presence of correspondingly non-uniform cell degradation effects. A determination of the local cell operation conditions is enabled by applying a segmented fuel cell assembly [1,4,5]. The current density distribution is proportional to the distribution of the electric output power of the active electrode region. Investigations made with the segmented single cell assembly enable an analysis of the interdependencies between local cell operating conditions and cell potentials. Fuel cell electrode regions where an undersupply with hydrogen is present can also be identified with a segmented fuel cell assembly. A measurement of the output current of a non-segmented cell only enables the calculation of an average cell current density by dividing the cell output current through the active electrode area.

It is not possible to distinguish between the anode and the cathode half-cell reaction with a segmented fuel cell assembly. This can only be achieved by introducing a constant potential into the test cell utilising a reference electrode. Anode and cathode potential can then be determined relative to this constant potential [6–10]. It is thus possible to sub-divide the overall electrochemical reaction into an anode and a cathode half-cell reaction. A local resolution of this sub-division into anode and cathode half-cell reactions is possible by integrating a number of reference electrode locations into the measurement assembly [11,12]. A total of four reference electrodes were installed with the design of the fuel cell assembly presented within this paper.

If a fuel cell is shut-down over a longer period of time, the flow field gas channels are normally exposed to the ambient air atmosphere. Anode and cathode flow fields are thus filled with ambient air. During start-up, hydrogen is fed into the anode flow field. The air is thus pushed out of the anode flow field by the stream of fresh hydrogen input gas. Regular operating conditions

* Corresponding author. Tel.: +43 316 873 8786; fax: +43 316 873 8782.
E-mail address: wr.baumgartner@gmx.at (W.R. Baumgartner).

0378-7753/$ – see front matter © 2008 Elsevier B.V. All rights reserved.
doi:10.1016/j.jpowsour.2008.01.001

with an electrochemical potential of 0 V (vs. NHE) are hence present in the anode flow field entrance region. The good electronic conductivity of the bipolar plates results in the formation of an almost uniform difference between the electric potentials of the anode and cathode bipolar plates. This difference in the electric potentials of the bipolar plates is also present in the flow field exit region, where the fuel cell is still operated in an air/air mode because the air has not yet been pushed out of the flow field by the fresh hydrogen supply.

The availability of oxygen in the anode electrode domain results in an oxygen reduction reaction (ORR) potential of roughly 1 V. The potential difference of approximately 1 V between the cathode and anode electrode is determined by the well-supplied flow field entry region. The cathode potential also has to be approximately 1 V higher than the anode electrode potential in the outlet region despite of the fact that the anode is still filled with air, shown in Fig. 1. High cathode potentials are therefore present with the outlet region. Investigations have already been made in order to demonstrate this effect [2].

The authors applied two separate fuel cells and operated one cell in hydrogen/air and the other cell in air/air mode.

Air/air regions can also be formed if the fuel cell is operated with small stoichiometries and small current densities. In this case, the small input gas flow rates can lead to some electrode regions being undersupplied. An undersupply of certain fuel cell electrode regions can also be caused by an accumulation of liquid water droplets within the flow field gas channels.

Dead-end operation of a fuel cell results in high overall energy conversion efficiencies and is therefore particularly relevant with stationary applications. Dead-end operation is made by closing the anode flow field exit and re-supplying the hydrogen consumed by the anode electrode reaction at a constant gas-phase pressure.

Nitrogen permeating through the membrane from the cathode into the anode domain accumulates within the anode electrode domain. Liquid water can also accumulate within the anode domain with certain operating conditions. This accumulation of nitrogen and (liquid) water can eventually lead to a hydrogen undersupply of certain anode electrode regions. This undersupply can result, as mentioned above, in a non-uniform current density distribution and high cathode potentials.

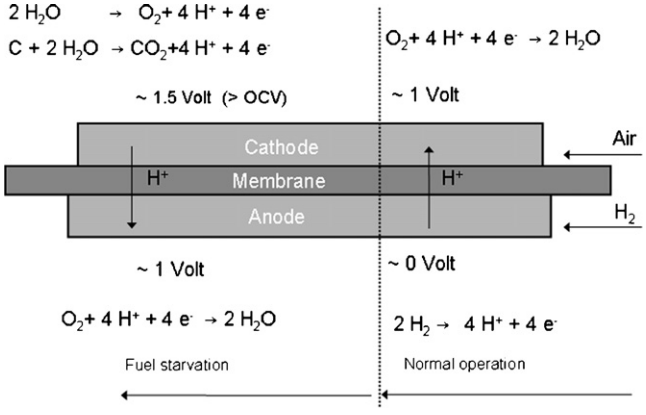

Fig. 1. Formation of high cathode potentials due to hydrogen undersupply [2].

Local electrochemical potentials measured in a single cell assembly are presented within this paper. A special emphasis was put on designing a test cell assembly that matches the state-of-the-art in PEMFC performance and design. The fuel cell assembly PEMFC CDL REF2, designed according to the requirements formulated above, was applied in a number of investigations including dead-end operation and hydrogen undersupply operation. Electrode potentials measured during the aforementioned undersupply operation of the fuel cell are presented within this paper.

2. Experimental

2.1. Test rig design

All measurements were made with a fully automated test rig developed within the CD-Laboratory [4,13]. The test rig is capable of supplying mixtures of hydrogen, nitrogen, oxygen and air utilising mass flow controllers (MFCs). Bubble humidifiers are utilised for fuel cell input gas humidification; humidity levels are checked with downstream humidity sensors. The system pressure can be varied between ambient pressure and 2 bara operation.

Electric properties are measured with a Zahner Elektrik impedance measurement station (IM6ex combined with PP240). Electrochemical potentials are measured utilising a USB multiplexer card from National Instruments (NI USB-6218). Thus, anode and cathode potentials can be measured in parallel at sample rates of 250 ms (4 Hz).

Fuel cell off-gases are fed into an online gas analysis station from Hartmann & Brown which allows detection of carbon monoxide, carbon dioxide, oxygen and hydrogen.

2.2. The PEMFC CDL REF2

A number of 25 cm^2 fuel cell assemblies for PEMFC cells were developed within the Christian Doppler Laboratory for Fuel Cell Systems (PEMFC CDL V1–V3 [4]).

The flow field design utilised with each of these cell assemblies is a triple serpentine with four gas channels located in parallel. This design provides a sufficient pressure drop between inlet and outlet to remove the reaction product water out of the cell. Cooling channels are installed into the carbon flow field plates, providing a convenient temperature control of the fuel cell applying water as heat transfer medium.

The system is sealed with two silicon seals with a thickness of 180 μm each installed between the carbon plates. The assembly is fixed with six screws and disc springs in order to provide a uniform and reproducible compression force over the complete cell area. The PEMFC CDL REF2 design has been developed from the previous PEMFC CDLV2 design. The same cell assemblies were also utilised as a basis for developing a segmented cell design and a short-stack [4,5,14]. All of these designs are based on one common platform; the different types of cell assemblies can therefore be arbitrarily combined. This flexibility with respect to the test cell configuration provides the possibility of inves-

tigating degradation effects in PEMFCs in many different ways.

It has been previously stated in scientific publications that it is almost impossible to measure the potential of PEMFC membranes in the middle of the membrane (i.e. in between the anode and cathode electrode).

Simulations reveal the interdependencies between size and orientation of the electrodes and the cell potential measured in the middle of the membrane [15–18]. If the potential is measured in a certain distance from the edges of the electrodes, a uniform membrane potential can be measured; this distance is at least 1.5 times the thickness of the membrane [19,20]. This membrane region is therefore referred to as the region of constant potential (RCP).

By intentionally increasing the size of one of the electrodes, the potential of the RCP is shifted towards the potential of the counter electrode [16,20].

The RCP can then be connected to an external reference electrode with a small strip of membrane [17]. Shifting the RCP towards the anode potential suggests itself with PEMFCs, as the anode electrode kinetics are significantly better than the cathode electrode kinetics, and the measured potential is therefore only subject to smaller variations than it would be the case if the cathode electrode potential would be measured.

Displacement factor is derived as the ratio of electrode offset δ and electrolyte thickness. Applying a displacement factor larger than three assures that the RCP is determined by the anode electrode potential. This corresponds to an electrode offset of 150 μm [16,20].

Due to manufacturing and assembling tolerances, an electrode offset of 1.25 mm was chosen with the measurements presented within this paper. The risk of using such a comparably large inactive anode electrode region is that a mixed potential may be formed due to the presence of oxygen diffusing through the membrane. The seal was therefore well adapted in the anode electrode domain to specifically address this problem.

A small strip of membrane is pressed onto the anode side of the membrane. This strip of membrane is stuck through a hole drilled into seal and carbon plate and into a 2 ml reservoir of 0.1 M sulfuric acid with a mercury sulfate reference electrode obtained from Schott Instruments GmbH, as shown in Figs. 2 and 3. The strip of membrane is humidified with distilled water to prevent it from drying out.

2.3. Analysis of the potentials

The electrochemical potentials of a cell have to be determined by measuring the electronic potentials.

Potentials are determined by measuring the stream of electrons with an appropriate instrument. This implicitly contains a problem for investigations with electrochemical systems. In electrochemical systems, it would be necessary to determine the potential within the electrolyte. A simplification is thus made in order to be able to apply electrical principles – in this case the calculation principles for impedances as well as the Ohm's law – in electrochemical applications. This assumption is that

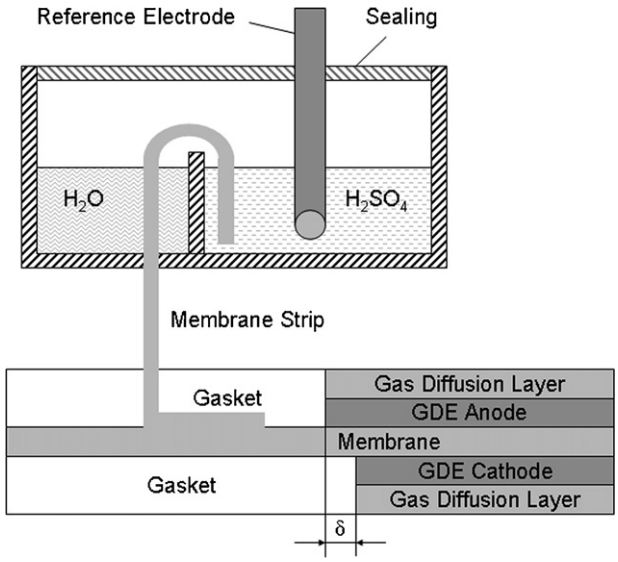

Fig. 2. Structure of the MEA and connection to membrane potential with the reference electrode.

the voltage drop over the electrolyte of an electrochemical cell is proportional to the electrical current.

Some inaccuracies are also detected in investigation applying electrochemical impedance spectroscopy (EIS) to electrochemical cells. The impedance of an electrochemical system is not necessarily equivalent to the impedance of a normal electrical circuit. Electrochemical impedances can show – in contrast to what is possible with regular electrical impedances – a current-dependent behaviour. The value of impedance therefore does not only depend on the frequency, but also on the current.

The measurement of the electrochemical potentials is described in the schematic of the equivalent circuit model presented in Fig. 4. It is thus possible to identify the problems of the measurement. A simplified representation of the anode and cathode half-cell reactions as individual voltage sources is applied.

A measurement relative to a common reference point is necessary in order to be able to distinguish between anode and cathode potentials. This reference point has to be located in between the anode and cathode electrodes and connected to the reference electrode.

The necessity of consecutively measuring the anode and the cathode potential can be derived from Kirchhoffs' law. A switch is therefore required to measure the two voltages with a small delay in time in between the individual measurements. If this

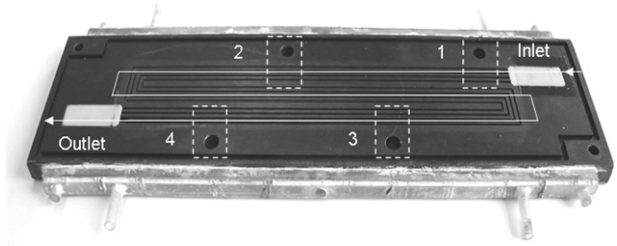

Fig. 3. Flow field and positions of the reference electrodes [21].

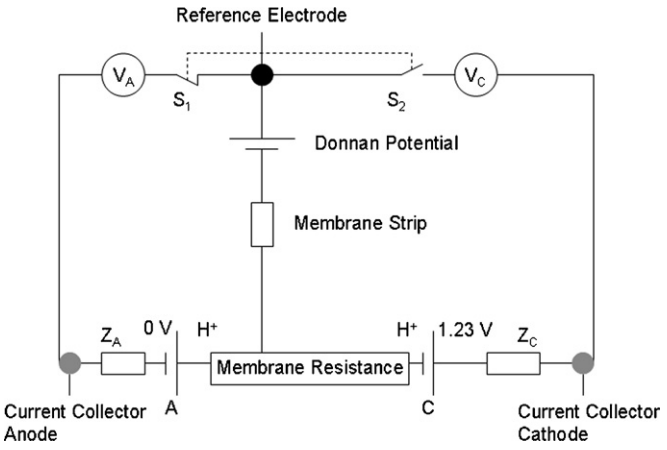

Fig. 4. Schematic of an equivalent circuit of the measurement setup.

switch would not have been included, the overall voltage would be divided by two due to the identical potentiometers if the membrane strip resistance is high. The actual cathode voltage can only be determined by applying a number of corrections that are inevitably linked to inaccuracies. The first voltage drop is due to the overvoltage within the GDE. The voltage drop in the measurement device as well as within the strip of membrane is – due to high internal resistance (10 GΩ) and the small voltage drops – in the order of μV.

The contact resistance between the membrane strip and the membrane can also be neglected due to the small measuring currents. A determination of the resistance of the membrane strip is not possible because the magnitude of the resistance is very small. The voltage drop across the membrane can be estimated according to Ohm's law and is therefore assumed to be linearly proportional to the current. A voltage correction therefore has to be applied if the cathode electrode potential is to be determined. The respective values are given in Table 1 and show the maximum potential correction for the total cathode. The actual potential of the total cathode electrode can thus be derived by adding the respective values. Locally resolved cathode potentials can be defined only by measuring the local membrane resistance and the current density distribution. These require an appropriate measuring equipment.

For these reasons, the authors decided not to apply the voltage correction to the measured values due to the immanent inaccuracies of the measurement setup as well as the aforementioned considerations with respect to an application of electrical impedance calculation principles with electrochemical systems.

Table 1
Membrane resistance of 5.67 mΩ and currents of 1–40 A

I (A)	E (mV)
1	0.006
5	0.028
10	0.057
20	0.113
30	0.170
40	0.227

The measured values are hence only corrected by subtracting the 650 mV of the mercury sulphate reference electrode versus NHE.

3. Results

3.1. Standard fuel cell operating mode

The cell assembly with integrated reference electrode was first operated under standard conditions in order to investigate the quality of the cell design and the accuracy of the measurement. The cell was thus operated with an anode stoichiometry of 1.5 and a cathode stoichiometry of 2.2 at a cell temperature of 70 °C. The fuel cell input gases were humidified in the bubble humidifiers and supplied to the cell at a relative humidity of 90%. The cell current was measured with the current collectors and therefore only provides an area-averaged value of the current density. A locally resolved analysis of the current density distribution is not possible. Utilising the reference electrode, the anode and cathode potentials can be analysed at four different locations of the active electrode area (see Fig. 3). Due to the fact that the reference electrode is contacted to the membrane region having approximately the anode electrode potential, a higher degree of inaccuracy is present with the measurement of the cathode electrode potential due to the resistance of the membrane. The actual cathode potential can therefore be estimated by adding the membrane resistance, as outlined above.

The impedance spectrum of the PEMFC CDL REF2 is shown in Fig. 5. The left intersection between the impedance curve and the real axis represents the high frequency resistance (HFR). The HFR corresponds to the ohmic resistance and can be primarily attributed to the membrane resistance in fuel cells. The ohmic resistance determined with the impedance spectrum shown in Fig. 5 can thus be determined as 5.67 mΩ.

A maximum voltage drop due to the resistance of the membrane of 227 mV can be derived from the values given in Table 1.

The potentials of the anode and cathode electrodes are measured at four different locations. The differences between the averaged cell voltage and the individual measurements can be

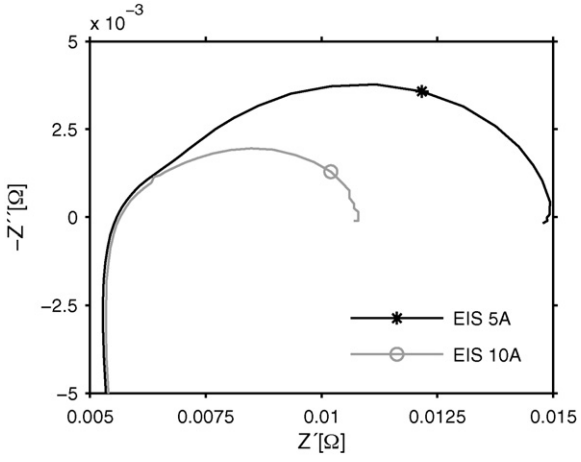

Fig. 5. Nyquist-plot for the measured impedance of the fuel cell; galvanostatic operation at 5 A and 10 A. 70 °C, hydrogen/oxygen.

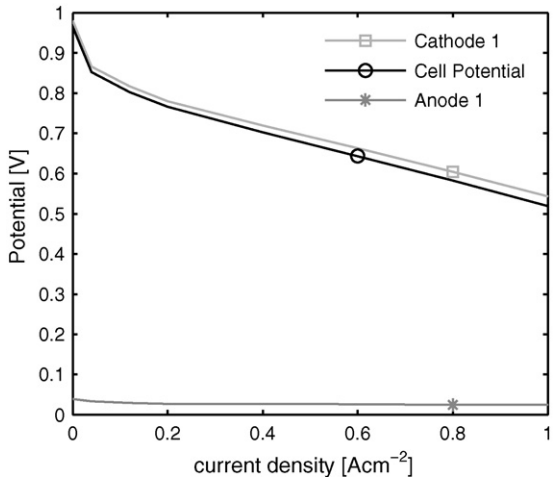

Fig. 6. Comparison of the cell voltage and the electrode potentials.

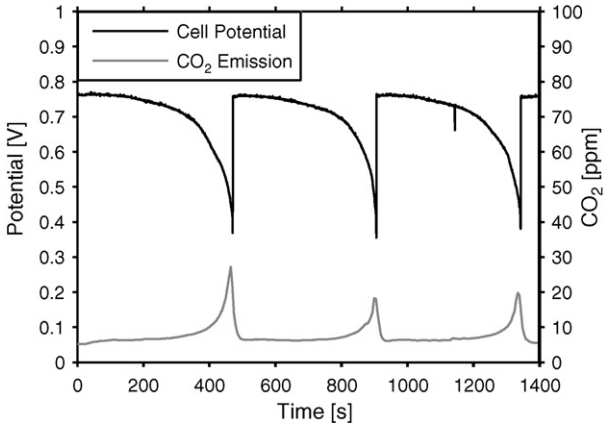

Fig. 7. Measurement of cell voltage and cathode off-gas during dead-end operation.

explained by additional voltage drops (e.g. in the carbon plates) as well as by the low local resolution of the measurements. The electrode potentials of the cell for a typical polarization curve are presented in Fig. 6. The measurements were made at standard conditions as explained before.

3.2. Dead-end operation

The cell was operated galvanostatically at a cell current of 10 A and air at a stoichiometry of 2.2 and 90% r.H. at a cell temperature of 70 °C. In order to prevent fatal cell degradation, the anode was purged when the entire cell potential was below 0.4 V.

These investigations were made with dry hydrogen input gas to avoid an accumulation of (liquid) water within the anode flow field gas channels resulting; this would potentially subject some electrode regions to an undersupply with fresh hydrogen. The supply with hydrogen has to be made in a way that the fuel cell is not damaged due to a rapid change in gas-phase pressure when the anode outlet is opened. The cathode off-gas is analysed during the dead-end operation cycle.

The variation of cell output voltage with time at dead-end operation is presented in Fig. 7. The cell voltage is thus drastically reduced even after short periods of dead-end operation due to the accumulation of nitrogen and water within the anode flow field domain. These effects occur because of the concentration difference between the cathode gas and the anode gas. In the case of long purge periods, the increased concentration of nitrogen and water at the anode results in a low hydrogen partial pressure and therefore high overvoltages [22]. Accumulation effects within the anode flow field also lead to strongly non-uniform current density distributions [4].

An anode that is subject to undersupply conditions is locally operated with very high relative current densities which can result in local cell degradation and ageing effects. The cathode off-gas shows an increase in the CO_2 content during dead-end operation, as presented in Fig. 7. CO_2 production could be caused by the aforementioned high cathode potentials due to hydrogen undersupply conditions. Roen et al. showed the influence of platinum on the corrosion of carbon support at different potentials [23]. They showed that the potential stability of the gas diffusion electrodes decreases in the presence of platinum catalysts. The carbon support stability, of the MEA used in the experiments discussed in this paper was investigated at different cell potentials in a previous paper [24]. This experiment was made at hydrogen/nitrogen conditions without oxygen gas supply. It was shown that oxygen from water electrolysis reacts with carbon at cell potentials above 0.9 V. At cell potentials above 1.4 V the carbon corrosion increases significantly [24].

A second effect causing CO_2 emissions could be high local cell currents, again resulting in degradation effects. It is beyond the scope of this publication to investigate to what degree both effects contribute to the overall CO_2 emissions of the fuel cell. Investigations on a combination of locally resolved current density distribution and electrode potentials measurements are currently being made.

The electrode potentials measured near the flow field input region show straight-forward characteristics. At measurement position 1, the overvoltages of the cathode electrode are increased when the cell is switched to dead-end operation (Fig. 8). This can be explained by high current densities at the hydrogen inlet region, as shown in a previous investigation [4]. At measurement position 2, a significantly different – but nevertheless reproducible – behaviour of the cathode electrode is measured as shown in Fig. 8. The overvoltage of the cathode electrode is reduced, and the overvoltage of the anode electrode is significantly increased particularly shortly before the cell has to be purged. This indicates that undersupply phenomena are present with this anode electrode region. The cathode potential is thus shifted to higher values which can also be seen in Fig. 8.

At measurement position 3 the anode overvoltage is increased even sooner than with measurement position 2, with the cathode potential being increased correspondingly (cp. Fig. 8 with Fig. 9). The cathode overvoltage even reaches a maximum potential and is subsequently slightly reduced just before the cell has to be purged. The anode potential is continuously increased throughout the dead-end operation period. This shift in the anode potential is again assumed to be linked to undersupply phenomena.

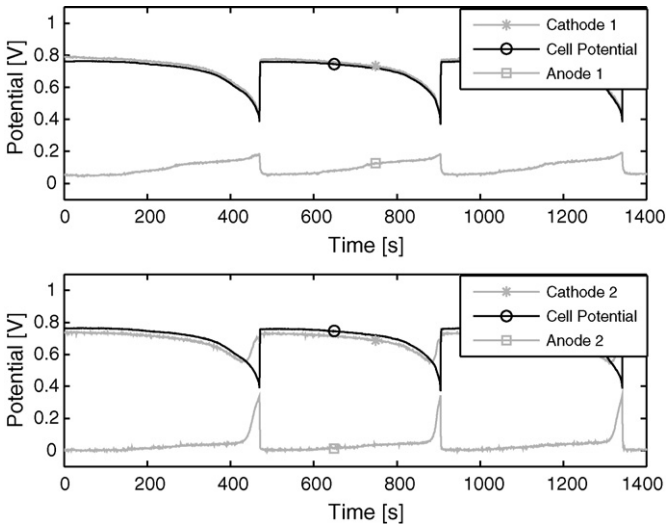

Fig. 8. Measurement of anode and cathode potentials at positions 1 and 2 during dead-end operation.

The same characteristics can also be seen with the measurements made in position 4.

The characteristics of a dead-end operation period can essentially be sub-divided into three domains. The first domain corresponds to an increase of the anode overvoltage. The second domain indicates the presence of strong undersupply phenomena. And the third domain indicates that a combination of undersupply phenomena and carbon corrosion rapidly increases the electrode potentials.

The following cell behaviour can be derived from the measurements. The entrance region of the cell is subject to regular fuel cell operation (see Fig. 1); the overvoltages increase as the local current densities are increased as shown in Fig. 10. The cathode potential is significantly higher at positions 3 and 4; this indicates that a small relative current density is present with these electrode regions [1,4]. This reduction in relative current densities is caused by the presence

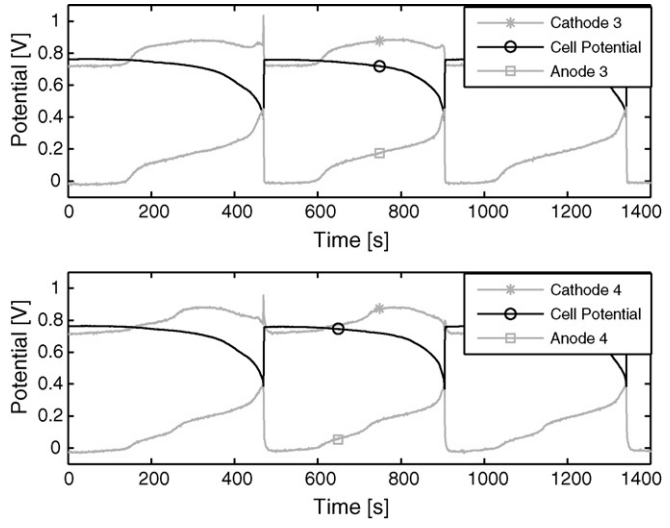

Fig. 9. Measurement of anode and cathode potentials at positions 3 and 4 during dead-end operation.

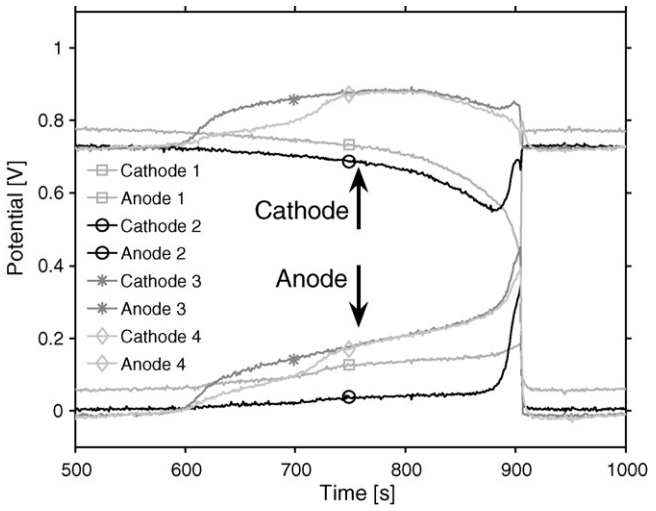

Fig. 10. Comparison of electrode potentials at positions 1–4 during dead-end operation.

of significant undersupply conditions in the anode electrode domain.

3.3. Hydrogen starvation

For this experiment the air was supplied with 90% r.H. and a stoichiometry of 2.2 at a cell temperature of 70 °C. During the experiments the cell was operated galvanostatically at 5 A. The hydrogen stoichiometry was progressively reduced from an initial value of $\lambda = 1.5$ down to $\lambda = 0.95$. The cell was operated for 3 min with each stoichiometry in order to reach stable operating conditions. Cell output voltage and electrode potentials as well as the off-gases were measured. Nitrogen (200 ml min^{-1}) has to be added to the anode gas in order to be able to measure the off-gas with the online GC.

The cathode off-gas at a hydrogen stoichiometry of $\lambda = 0.95$ surprisingly contains hydrogen, whereas the anode off-gas contains some CO_2. This can be explained by local high current densities and high cathode potentials as mentioned above.

A significant increase in the cathode electrode potential up to 1500 mV can be derived from the plot shown in Fig. 11. This potential is close to the electrolysis potential of water and therefore explains the hydrogen content of the cathode off-gas as shown in a second hydrogen undersupply experiment presented in Fig. 12. At galvanostatic operation the missing protons have to be produced by water electrolysis on the anode side. Electrolysis of water does not only explain the presence of hydrogen in the cathode off-gas, but also the presence of carbon dioxide in the anode off-gas. Due to the presence of oxygen and catalyst at the cathode side, the hydrogen formation is likely to be located near the gas outlet. The hydrogen is therefore unable to react and can be detected by the online gas analysis. Due to the fact that the measured cathode electrode potential is only a local potential, an even higher potential might be present in other regions of the cell. A reduction of the hydrogen stoichiometry results in an increase of the anode potential. A very significant increase of the anode potential is derived when the stoichiometry is reduced from $\lambda = 1.05$ to 1.0 and from $\lambda = 1.0$ to 0.95.

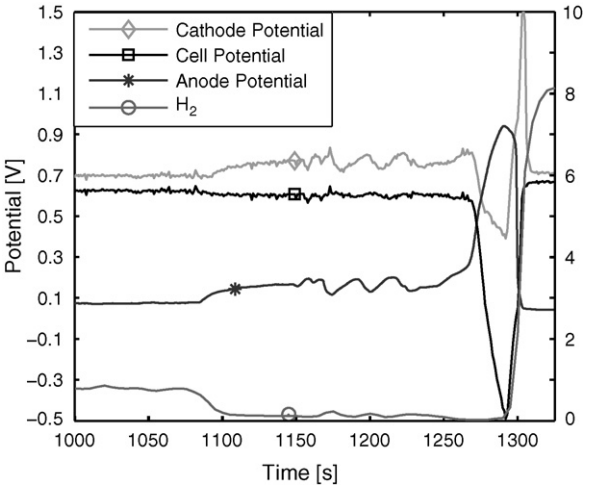

Fig. 11. Measurement of cell voltage, anode off-gas, anode and cathode potential at hydrogen starvation conditions.

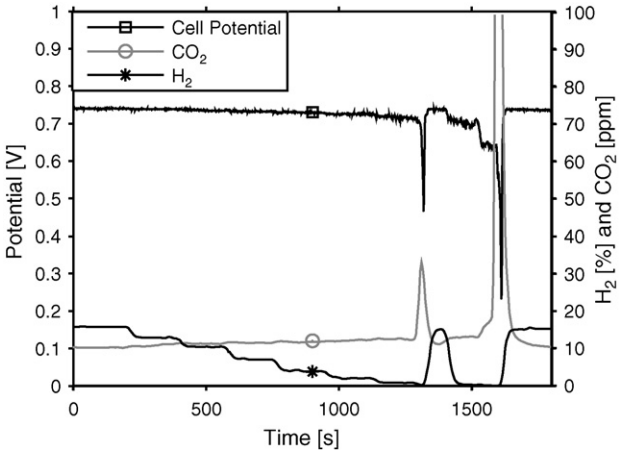

Fig. 13. Measurements of cell voltage and anode off-gas at hydrogen starvation conditions.

The cathode electrode potential is slightly increased with stoichiometries of around $\lambda = 1.0$, and is drastically reduced with stoichiometries of around 0.95.

The strong reduction in cell voltage is thus caused by a strong increase of the anode as well as the cathode overvoltages.

A strong increase of the anode electrode potential is already derived with stoichiometries of $\lambda = 1.0$. At $\lambda = 0.95$, a very strong increase in anode potential is derived. When the cell voltage approached negative values, the hydrogen stoichiometry was again set to a value of 1.5 to prevent the cell from being damaged.

Another measurement series was made with the cell being galvanostatically operated at 5 A. Nitrogen was again added to the anode input gas flow at a rate of 200 ml min^{-1} for the gas analysis system. The hydrogen stoichiometry was again reduced progressively until values smaller than one were reached. A local undersupply of the fuel cell was thus investigated. Fig. 13 presents an investigation where two hydrogen undersupply conditions were simulated, and the response of the cell was investigated. The first undersupply was made for 20 s, the second undersupply was made for 30 s. Fig. 13 shows a sharp drop in cell output voltage and a correspondingly sharp increase in CO_2 emissions at the anode.

The electrode overvoltage characteristics derived with this cell operation essentially follow the characteristics already derived for dead-end operation. Electrode potentials measured in the hydrogen inlet region are shown in Fig. 14.

The first drop in cell voltage was relatively short, and the anode and cathode overvoltages were therefore only slightly increased.

These changes in electrode potentials correspond to a normal change in cell current controlled by the galvanostatic operation of the cell. The second drop in cell voltage again results in an increase of the electrode overvoltages. Cell voltage and electrode potentials soon recover after feeding fresh hydrogen to the cell.

The anode electrode potential is significantly increased in positions 3 and 4, and the cathode electrode potential is also increased to values higher than those present with the initial

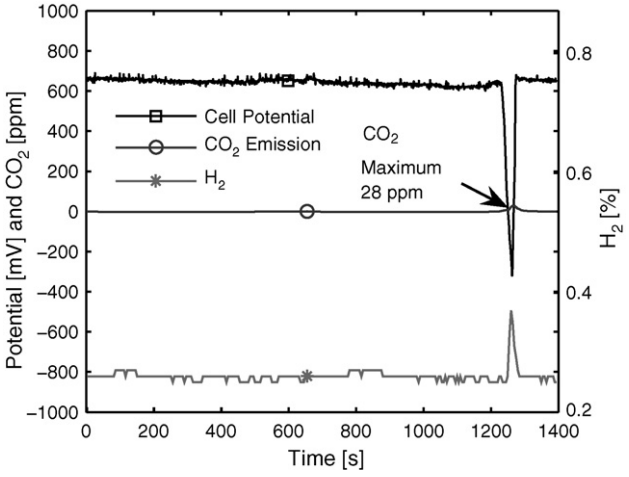

Fig. 12. Analysis of the cathode off-gas at different hydrogen stoichiometries.

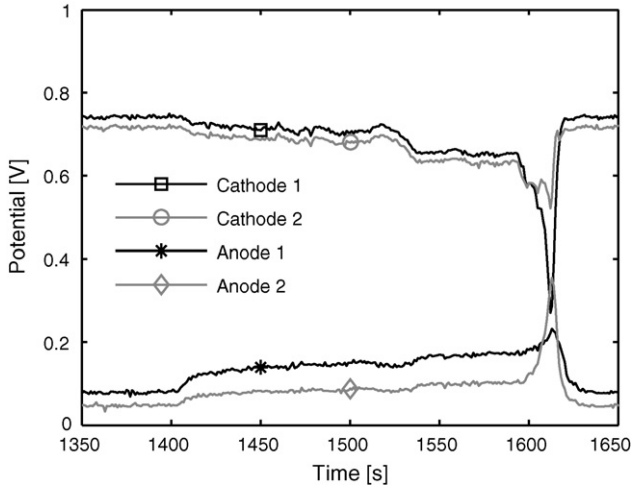

Fig. 14. Measurement of anode and cathode potential at positions 1 and 2 at hydrogen starvation conditions.

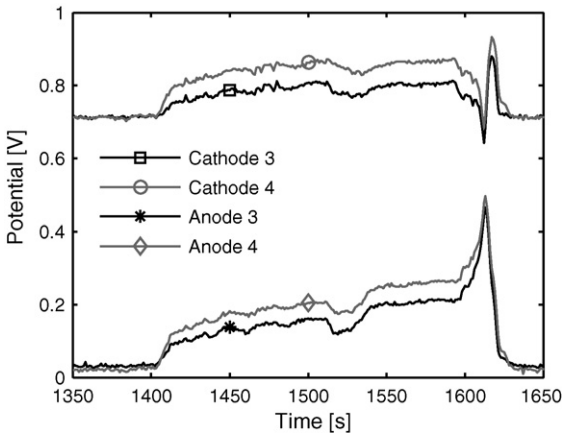

Fig. 15. Measurement of anode and cathode potential at positions 3 and 4 at hydrogen starvation conditions.

operating conditions of the cell before the hydrogen undersupply conditions as shown in Fig. 15. This electrode region therefore contributes a considerably smaller fraction of the cell output current due to the local hydrogen undersupply conditions.

The increase of the anode potential can be explained by the permeation of oxygen from the cathode and by local electrolysis. Particularly interesting is the short peak in cell voltage when the cell is being purged. During purging, the cell is subject to air/air operation, see Fig. 1 and high cathode electrode potentials are present for a couple of seconds (Fig. 15). These high cathode electrode potentials can result in carbon corrosion phenomena at the cathode electrode and thus an irreversible damage to the cell.

Cell operation with hydrogen undersupply conditions generally shows similar characteristics to dead-end operation. One remarkable effect is derived: the cathode electrode potential is significantly increased during purging for a couple of seconds. This is clearly an electrochemical effect and is not caused by measurement & instrumentation, as this effect would then have to be measured with all four reference electrodes. Due to the fact that the measured potentials only represent small fractions of the whole active electrode area of the cell, it would be possible that even higher values could be measured locally.

Measurements made with the laboratory-scale cell did not exceed 1.5 V. The gas analysis nevertheless documented the presence of strong degradation effects caused by the local undersupply with hydrogen.

Particularly the reversible thermodynamic potential of approximately 1.23 V is present within the cell during the measurement series. It was not possible to measure the potential directly with a high local resolution during fuel undersupply under load, though. Inaccuracies in the measurement & instrumentation hardware as well as the ohmic correction are possible explanations why this potential could not be measured. Another possibility would be that these potentials cannot be measured in a cell with such a non-uniform gas distribution. An improvement of the general approach in measuring the electrochemical potentials with high resolutions is thus required.

4. Conclusions

Electrode potentials are investigated during hydrogen undersupply operation of a PEMFC within this paper. Investigations were made with a laboratory-scale single cell assembly and dead-end operation as well as open-end operation at hydrogen undersupply conditions.

Hydrogen undersupply results in a non-uniform gas distribution within the cell. Some regions of the cell as thus subject to operation at undersupply conditions and do not contribute significantly to the overall cell output current. No critical electrode potentials were measured in the investigations presented within this paper under load operation. Only an abrupt increase of the hydrogen stoichiometry after a period of hydrogen undersupply operation results in a short presence of very high potentials at the cathode electrode. This effect will be particularly relevant for fuel cell systems during start-up and dead-end operation. The cathode electrode potential is then already in the order of 1 V and will then be increased to values even higher than those reported within this paper if the anode flow field is filled with hydrogen. Utilising appropriate shut-down and start-up procedures will reduce this effect.

Due to the fact that actual fuel cell systems will most likely have to be operated in parallel to batteries, the danger of facing cell voltages in excess of the OCV is limited. During operation, the fuel cell will normally not be operated with near-OCV cell voltages due to the fact that parasitic loads such as the compressor will have to be operated by the fuel cell. The cathode electrode potential will thus also be correspondingly smaller than in OCV mode.

In order to be able to investigate the effects of fuel cell operation with hydrogen undersupply conditions quantitatively, a segmented cell with reference electrodes is currently being developed. This setup will combine the possibility of investigating locally resolved current density distributions and electrode potentials.

References

[1] Z. Liu, L. Yang, Z. Mao, W. Zhuge, Y. Zhang, L. Wang, J. Power Sources 157 (2006) 166–176.
[2] H. Tang, Z. Qi, M. Ramani, J.F. Elter, J. Power Sources 158 (2006) 1306–1312.
[3] A. Taniguchi, T. Akita, K. Yasuda, Y. Miyazaki, J. Power Sources 130 (2004) 42–49.
[4] W.R. Baumgartner, Dissertation, TU Graz, 2007.
[5] T. Traußnig, Diploma Thesis, TU Graz, 2006.
[6] J. Ihonen, F. Jaounen, G. Lindbergh, An Lundblad, G. Sundholm, J. Electrochem. Soc 149 (4) (2002) A448–A454.
[7] Z. Siroma, R. Kakitsubo, N. Fujiwara, T. Ioroi, S. Yamazaki, K. Yasuda, J. Power Sources 156 (2006) 284–287.
[8] G. Li, P.G. Pickup, Electrochem. Acta 49 (2004) 4119–4126.
[9] M. Kunimatsu, H. Qiao, T. Okada, J. Electrochem. Soc. 152 (5) (2005) E161–E166.
[10] G. Li, P.G. Pickup, Electrochem. Solid State Lett. 9 (5) (2006) A249–A251.
[11] K. Mitsuda, T. Murahashi, J. Electrochem. Soc. 137/10 (1990).
[12] Z. Siroma, J. Takahashis, K. Yasuda, K. Tanimoto, M. Inaba, A. Tasaka, ECS Trans. 3 (1) (2006) 1031–1040.
[13] W.R. Baumgartner, Diploma Thesis, TU Graz, 2004.
[14] B. Hebenstreit, Diploma Thesis, TU Graz, 2007.

[15] M. Strähler, FZJ, Energy Technology, vol. 47, ISBN: 3-89336-428-5 (2005).
[16] S.B. Adler, B.T. Henderson, M.A. Wilson, D.M. Taylor, R.E. Richards, Solid State Ionics 134 (2000) 35–42.
[17] W. He, T. Van Nguyen, J. Electrochem. Soc. 151 (2) (2004) A185–A195.
[18] U. Landau, N.L. Weinberg, E. Gileadi, J. Electrochem. Soc. 135/2 (1988).
[19] S.B. Adler, J. Electrochem. Soc. 149 (5) (2002) E166–E172.
[20] Z. Liu, J.S. Wainright, W. Huang, R.F. Savinell, Electrochem. Acta 49 (2004) 923–935.
[21] P. Parz, Diploma Thesis, TU Graz, 2008.
[22] S. Hikita, F. Nakatani, K. Yamane, Y. Takagi, JSAE Rev. 23 (2002) 177–182.
[23] L.M. Roen, C.H. Paik, T.D. Jarvi, Electrochem. Solid State Lett. 7 (2004) A19–A22.
[24] W.R. Baumgartner, E. Wallnöfer, Th. Schaffer, V. Hacker, P. Peinecke, P. Prenninger, ECS Trans. 3 (1) (2006) 811.